arXiv:1606.08608v1 [astro-ph.GA] 28 Jun 2016

CCD UBV Photometry and Kinematics of the Open Cluster NGC 225

Selçuk Bilir[a,*], Z. Funda Bostancı[a], Talar Yontan[b], Tolga Güver[a], Volkan Bakış[c], Tansel Ak[a], Serap Ak[a], Ernst Paunzen[d], Zeki Eker[c]

[a]*Istanbul University, Faculty of Science, Department of Astronomy and Space Sciences, 34119 University, Istanbul, Turkey*
[b]*Istanbul University, Graduate School of Science and Engineering, Department of Astronomy and Space Sciences, 34116, Beyazıt, Istanbul, Turkey*
[c]*Department of Space Sciences and Technologies, Faculty of Sciences, Akdeniz University, Antalya 07058, Turkey*
[d]*Department of Theoretical Physics and Astrophysics, Masaryk University, Kotlářská 2, 611 37 Brno, Czech Republic*

Abstract

We present the results of CCD UBV photometric and spectroscopic observations of the open cluster NGC 225. In order to determine the structural parameters of NGC 225, we calculated the stellar density profile in the cluster's field. We estimated the probabilities of the stars being physical members of the cluster using the existing astrometric data. The most likely members of the cluster were used in the determination of the astrophysical parameters of the cluster. We calculated the mean radial velocity of the cluster as $V_r = -8.3 \pm 5.0$ km s^{-1} from the optical spectra of eight stars in the cluster's field. Using the $U-B$ vs $B-V$ two-colour diagram and UV excesses of the F-G type main-sequence stars, the reddening and metallicity of NGC 225 were inferred as $E(B-V) = 0.151 \pm 0.047$ mag and $[Fe/H] = -0.11 \pm 0.01$ dex, respectively. We fitted the colour-magnitude diagrams of NGC 225 with the PARSEC isochrones and derived the distance modulus, distance and age of the cluster as $\mu_V = 9.3 \pm 0.07$ mag, $d = 585 \pm 20$ pc and $t = 900 \pm 100$ Myr, respectively. We also estimated the galactic orbital parameters and space velocity components of the cluster and found that the cluster has a slightly eccentric orbit of $e = 0.07 \pm 0.01$ and an orbital period of $P_{orb} = 255 \pm 5$ Myr.

*Corresponding author
Email address: sbilir@istanbul.edu.tr (Selçuk Bilir)

Keywords: Galaxy: open cluster and associations: individual: NGC 225, stars: Hertzsprung Russell (HR) diagram

1. Introduction

NGC 225 ($\alpha_{2000.0} = 00^h43^m39^s, \delta_{2000.0} = +61°46'30''$; $l = 122°.01$, $b = -1°.08$; WEBDA database[1]) is a sparsely populated and not a well-studied open cluster. Its age determined by Lattanzi et al. (1991) from photographic measurements and a recently revised study by Subramaniam et al. (2006) do not agree with each other. The limited number of observations, which are from older photographic measurements and some 2MASS data, motivated us to observe and study NGC 225 by contemporary CCD technology at optical wavelengths.

Proper motions and approximate photographic visual magnitudes of the stars in the field of NGC 225 were first given by Lee (1926). First precise UBV photographic and photoelectric measurements of the cluster were performed by Hoag et al. (1961), who also constructed V vs $B-V$ colour-magnitude (CMD) and $U-B$ vs $B-V$ two-colour diagrams (TCD). Johnson et al. (1961) measured the reddening for the cluster as $E(B-V) = 0.29$ mag using the data presented by Hoag et al. (1961). Svolopoulos (1962) determined the spectral classes for a number of stars in the field of the cluster, for which the photoelectric magnitudes were already given by Hoag et al. (1961), and measured the reddening, the distance modulus and the distance of the cluster as $E(B-V) = 0.29$ mag, $(m-M) = 9.0$ mag and $d = 630$ pc, respectively. Hoag & Applequist (1965) measured H_γ equivalent widths of the brighter stars in the field of the cluster photoelectrically and determined their spectral classes. The distance modulus of the cluster were estimated as $(m-M) = 9.1$ mag. But, later when Becker & Fenkart (1971) catalogued open clusters its distance was re-established again, where the reddening, uncorrected the distance modulus, the distance and the apparent diameter of the cluster were given as $E(B-V) = 0.29$ mag, $(m-M) = 9.87$ mag, $d = 630$ pc and $D = 14$ arcmin, respectively. Lattanzi et al. (1991) investigated NGC 225 in detail and determined 28 probable member stars of the cluster according to the proper motions measured in their study. They had used the photographic plates taken in B and V bands for estimating its age,

[1] webda.physics.muni.cz

reddening and distance as $t = 120$ Myr, $E(B-V) = 0.25 \pm 0.08$ mag and $d = 525 \pm 73$ pc, respectively. Almost one and a half decades later, the cluster was studied by Subramaniam et al. (2006), who re-estimated the cluster parameters using photographic UBV and Two Micron All Sky Survey's JHK_s photometry ($2MASS$, Skrutskie et al., 2006). Subramaniam et al. (2006) estimated the age of the cluster differently as $t = 0.5 - 10$ Myr and argued that its age is not 120 Myr as already suggested by Lattanzi et al. (1991). Strengthening this conclusion they proposed that two Herbig Be stars with H_α emission, dust lanes and nebulosity exist in the vicinity of the cluster implying possible results of recent star formation.

In this study, we report our conclusions extracted from our CCD UBV observations of NGC 225. Our report includes the mean radial velocity (RV) of the cluster measured from low-resolution optical spectra of some brighter stars of NGC 225. From these data, we have calculated the cluster's astrophysical and kinematical parameters. Using the proper motions of the stars, we have estimated their probabilities of being physical members of the cluster. We find the reddening and metallicity of the cluster following two independent methods. Its distance modulus and age were inferred by fitting stellar isochrones to the observed CMDs, while keeping the reddening and metallicity constant (Bilir et al., 2010; Yontan et al., 2015; Bostancı et al., 2015; Ak et al., 2016).

We have summarized the observations and the data reductions in Section 2. The CMDs, structural parameters of NGC 225, and the membership probabilities of the stars in the cluster field were presented in Section 3. In Section 4, we measure the astrophysical parameters of the cluster. Section 5 discusses the results.

2. Observations

2.1. Photometry

CCD UBV observations of NGC 225 were carried out on 18th July 2012 using the 1m Ritchey-Chrétien telescope (T100) located at the TÜBİTAK National Observatory (TUG)[2] in Bakırlıtepe, Antalya/Turkey. A composite V-band image taken with a total exposure time of 30 s is shown in Fig. 1. Fig. 1 also shows an image obtained from 2MASS with the same field of

[2]www.tug.tubitak.gov.tr

Table 1: Exposure times for each passband. N denotes the number of exposure.

Filter	Exp. time (s)×N
U	180×3 , 30×3
B	30×3 , 3×3
V	10×3 , 1×3

view. Dust lanes surrounding BD +61 154 to the upper side of the 2MASS image can be seen while it is not present in our V-band image. Since CCD UBV images of NGC 225, NGC 6811 and NGC 6866 were taken by T100 in the same night, the details of the observations and photometric reductions can be found in Yontan et al. (2015) and Bostancı et al. (2015), where the photometric analyses of NGC 6811 and NGC 6866 are discussed, respectively. Below, a brief summary is given.

Images of the cluster's field were acquired with the UBV filters with short and long exposures to cover the widest possible flux range. The night was moderately photometric with a mean seeing of $1''.5$. Exposure times for each passband are given in Table 1. IRAF[3], PyRAF[4], and astrometry.net[5] (Lang, 2009) were used for pre-reduction processes of images and transforming the pixel coordinates of the objects identified in frames to equatorial coordinates. The aperture photometry packages of IRAF were utilized to measure the instrumental magnitudes of the standard stars. From the observations of the standard stars (Landolt, 2009), atmospheric extinction and transformation coefficients for the observing system were determined through the equations given in Janes & Hoq (2013) and Ak et al. (2016). The coefficients for that particular night are listed in Table 2 of Yontan et al. (2015). We used Source Extractor (SExtractor)[6] and PSF Extractor (PSFEx) (Bertin & Arnouts, 1996; Bertin, 2011) together with custom written python and IDL scripts to detect and measure and catalog brightnesses of the objects within the cluster's field (Bertin & Arnouts, 1996). Aperture corrections were also applied

[3]IRAF is distributed by the National Optical Astronomy Observatories.

[4]PyRAF is a product of the Space Telescope Science Institute, which is operated by AURA for NASA

[5]http://astrometry.net

[6]SExtractor: Software for source extraction.

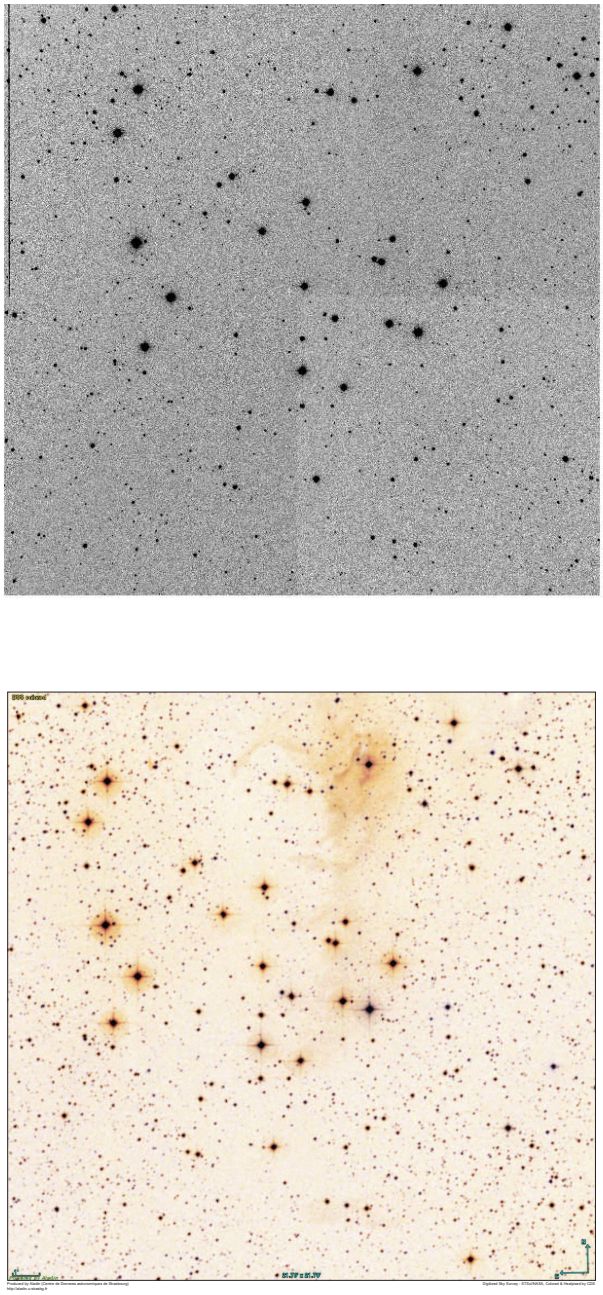

Figure 1: An inverse coloured composite V-band image of NGC 225 (*upper*) obtained with T100 telescope of the TÜBİTAK National Observatory. The integral exposure time and the field of view are 30 sec and about 21×21 arcmin, respectively (North top and East left). A 2MASS composite image with the same size is also presented (*lower*).

to the instrumental magnitudes of the objects identified in the field. Instrumental magnitudes of the objects in the cluster field were transformed as described in Yontan et al. (2015).

2.2. Spectroscopy

The spectroscopic observations of the stars in the direction of NGC 225 were performed in two observing seasons between 2010 and 2011 using the TUG Faint Object Spectrograph and Camera (TFOSC) attached to the 1.5-m RTT150 telescope of TUG. It is possible with the TFOSC to obtain low resolution ($R \sim 500$) optical spectra in a single spectral order as well as medium resolution ($R \sim 5100$) echelle spectra of celestial objects in 11 spectral orders. During the observing campaign, we selected the grism 9 (335-940 nm) to obtain the highest possible resolution of ~ 5100. A pinhole with a diameter of 100 μm giving a spatial resolution of $1''.78$ were used at the focal plane of the telescope. For wavelength calibration, spectra of the Fe-Ar lamp were taken before and after each program star observation. We corrected the pixel to pixel variations (flat-fielding) using the halogen lamp spectra taken as a series in the beginning of each observing night. In order to standardize our RV measurements, we selected two standard stars (Vega and HD 693) and observed them together with the program stars. The reduction and analysis of the spectra were performed with the IRAF using the noao/echelle task. We obtained a total of 23 spectra of 21 program stars. The observing log is given in Table 2.

Spectral types of the program stars have been determined by means of matching the observed spectra with the high-resolution spectra available in the UVES Pop Library (Bagnulo et al., 2003). Before starting to match the spectra, the resolution difference between two data sets have been corrected. In order to do this, we have degraded the high-resolution UVES spectra by convolving a Gaussian ($G(\lambda) = 1/(2\pi\sigma^2)e^{\lambda^2/2\sigma^2}$), where $\sigma = 50$ was found to be best fitting to our spectra. The spectral types determined are listed in Table 2. In Fig. 2, we show some spectral regions of some selected program stars together with the best matching stellar spectra in the UVES library.

Optical spectra obtained in this study were also used to measure RVs of the stars in the direction of NGC 225. Before measuring RVs of the program stars, possible systematic errors in the RV measurements caused by the observing equipments were investigated by means of measuring the positions of the static lines in the spectra such as the positions of the telluric lines. We detected some unexpected Doppler shifts on the order of several

Table 2: Observing log and some basic information of the program stars for which optical spectra were taken in this study. The S/N ratio refers to the continuum near H_α. V_r represents the radial velocity. Equatorial coordinates, brigtneses and colours of the stars located out of our field of view were taken from the SIMBAD database and indicated with an asterisk symbol in the first column. Star names were taken from Lattanzi et al. (1991). So, LMM is the short for Lattanzi, Massone and Munari.

ID	Star	Other Name	α_{2000} (hh:mm:ss.ss)	δ_{2000} (dd:mm:ss.ss)	V (mag)	$B-V$ (mag)	SpT	Date (JD-2400000)	S/N	V_r (km s^{-1})
∗01	LMM 01		00 41 49.29	+61 59 02.71	11.320	0.500	A8IV	55800.5498	100	2.2
∗02	LMM 33		00 42 17.90	+61 59 35.94	12.370	0.800	B4V	55798.5729	50	-79.9
03	LMM 83		00 43 10.88	+61 47 19.05	10.130	0.570	B8V	55486.6114	190	-6.6
04	LMM 88	BD+60 86	00 43 18.23	+61 45 37.56	9.713	1.668	K2III	55486.5331	150	-129.0
05	LMM 92		00 43 25.63	+61 48 51.78	11.560	0.420	B9IV	55798.3811	80	-16.0
06	LMM 94	BD+60 87	00 43 26.58	+61 45 55.89	10.338	0.550	B8IV	55797.4427	150	-4.0
07	LMM 95		00 43 28.88	+61 48 04.15	10.940	0.250	A0IV	55797.5615	110	-4.3
08	LMM 96		00 43 31.00	+61 48 10.29	12.172	0.551	A5V	55799.3618	100	-13.4
09	LMM 98		00 43 36.94	+61 53 40.23	11.982	0.347	A4V	55798.5388	80	-7.1
10	LMM 113	BD+61 157	00 43 51.06	+61 50 08.44	10.630	0.280	B9V	55797.4726	130	-9.5
11	LMM 114		00 43 51.47	+61 47 13.54	10.890	0.230	B9V	55797.5251	150	0.4
12	LMM 115	BD+60 91	00 43 52.13	+61 44 18.04	9.873	0.961	G7IV	55486.4615	160	-168.2
13	LMM 127		00 44 12.81	+61 51 01.88	11.420	0.290	A0V	55800.5725	110	-17.4
14	LMM 132		00 44 16.53	+61 50 44.01	12.342	0.436	A5V	55799.4000	120	-16.1
∗∗15	LMM 149	BD+60 94	00 44 30.68	+61 46 49.94	9.640	0.120	B8V	55797.3182	170	-9.4
	LMM 149							55799.5555	160	-7.6
∗∗16	LMM 161	BD+61 162	00 44 40.46	+61 54 01.77	9.700	0.120	B9V	55797.3736	170	-1.2
∗∗17	LMM 163	BD+61 163	00 44 40.82	+61 48 43.32	9.280	0.130	B7IV-V	55797.2775	260	-16.3
	LMM 163							55799.5302	220	-9.8
18	LMM 170	BD+61 164	00 44 46.43	+61 52 31.52	10.004	0.149	B9V	55797.6211	240	-2.4
19	LMM 174		00 44 47.48	+61 56 49.42	11.608	0.386	A3IV	55798.4111	110	-14.7
20	LMM 197		00 45 08.38	+61 56 24.75	12.984	0.358	A7III-IV	55799.4357	100	-45.8
∗21	LMM 269		00 46 00.67	+61 44 14.55	11.190	0.260	A5V	55799.4990	170	-5.2

(*): These stars are not located in our field of view.

(**): These stars are not included in our photometric catalogue as they are saturated.

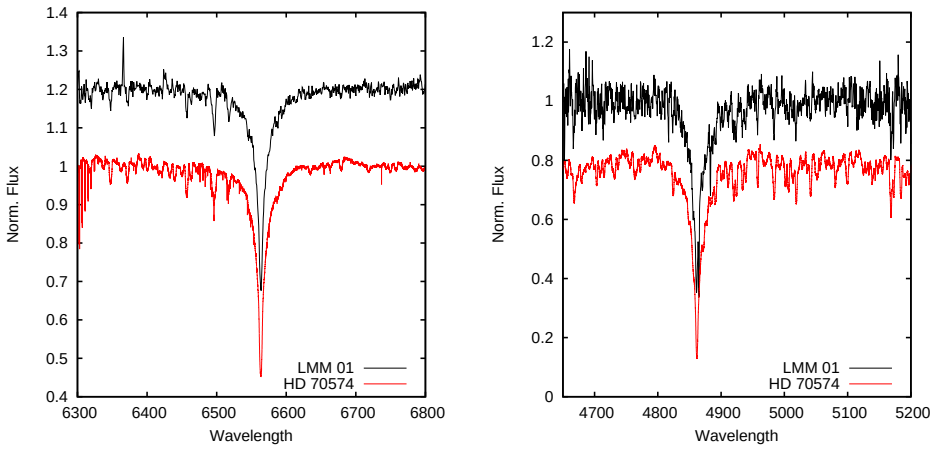

Figure 2: Two sample spectral regions of the selected program star and the degraded high-resolution stellar spectra of A8IV-type star HD 70574 in the UVES Pop Library.

tens of km s^{-1} due to the motion of the stars in the pinhole at very small seeing conditions and corrected these unexpected shifts by shifting spectra in the wavelength domain. After these corrections, the RVs of the program stars were measured by means of fitting Gaussian functions to the center of spectral lines in the *splot* task of IRAF. The uncertainty in the measurements is on the order of a few km s^{-1}, which is determined by the standard deviation of the subsequent measurements. However, we estimate an uncertainty of $\sim 5-9$ km s^{-1} for each measurement due to the low resolution of spectrograph. The list of RVs are given in Table 2.

3. Data analysis

3.1. Identification of stars and the photometric completeness

We identified 1382 sources in the field of NGC 225 and constructed a catalogue. The stellarity index (SI) provided by SExtractor was used to detect non-stellar objects, most likely galaxies, in our catalogue. The objects with SI smaller than 0.8 were assumed to be non-stellar sources and therefore removed from further analysis (Andreuzzi et al., 2002; Karaali et al., 2004). The resulting catalogue contains 1019 stars. Individual stars in the final

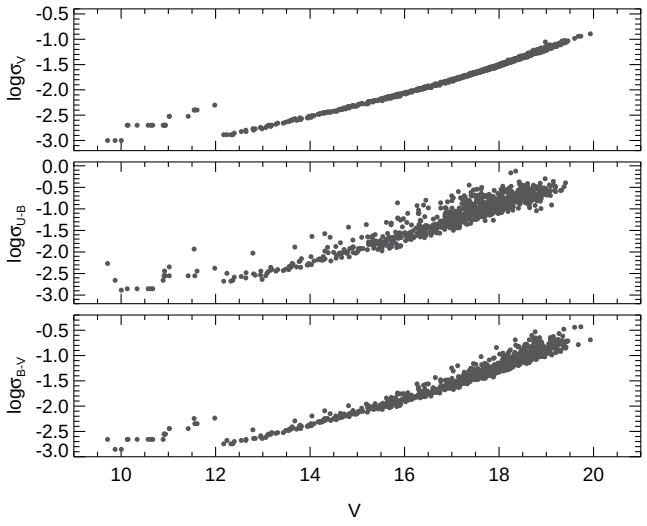

Figure 3: Colour and magnitude errors of the stars observed in the field of the open cluster NGC 225, as a function of V apparent magnitude.

photometric catalogue are tabulated in Table 3. The columns of the table are organized as equatorial coordinates, apparent magnitude (V), colours ($U-B$, $B-V$), proper motion components ($\mu_\alpha \cos\delta$, μ_δ) and the probability of membership (P). The proper motion components of the stars were taken from Roeser et al. (2010).

Fig. 3 shows the errors of the measurements in the V band, and $U-B$ and $B-V$ colours as a function of the apparent V magnitude. We listed the mean errors in the selected magnitude ranges in Table 4. Table 4 reveals that the errors are relatively small for stars with $V < 17$ mag, while they increase exponentially towards fainter magnitudes. As expected, the largest errors for a given V magnitude were found for the $U-B$ colours of the stars in the field. For stars brighter than $V = 17$ mag, the mean photometric errors in the V band and $B-V$ colour index are smaller than 0.012 and 0.021 mag, respectively. The mean errors in the $U-B$ colour index are smaller than 0.050 mag for stars brighter than the same V magnitude limit.

Since there is no previously available optical CCD photometry for NGC 225, we have compared our measurements (Fig. 4) with those of Lattanzi et al. (1991), who give photographic V-band magnitudes and $B-V$ colour indices

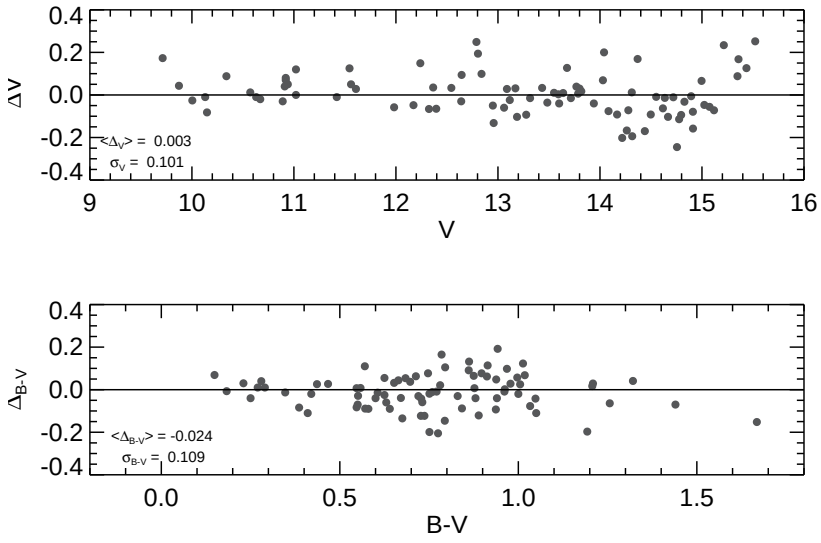

Figure 4: Comparison of the magnitudes and colours in this study with those of Lattanzi et al. (1991). The means and standard deviations of the differences are shown in the panels.

of some stars in the field of NGC 225, using 98 stars detected both in their study and ours. In Fig. 4, the values on the abscissa refer to our measurements, while the magnitude or colour differences in the ordinates present the differences between the two studies. The mean magnitude and colour residuals are calculated as $\langle \Delta_V \rangle = 0.003 \pm 0.101$ and $\langle \Delta_{B-V} \rangle = -0.024 \pm 0.109$ mag from the comparison. This comparison includes only stars cross-identified in the two studies and shows generally good agreement between them, although the magnitude and colour measurements in Lattanzi et al. (1991) are based on the photographic photometry for which relatively higher mean errors and disagreements with the CCD photometry due to different photographic and CCD passbands could be expected.

We determined the photometric completeness limit of the data since it can be very important in the reliable calculation of the astrophysical parameters of the cluster. In order to find this limit, we constructed a histogram of V magnitudes and showed it in Fig. 5. As the mode of the distribution of V magnitudes is 18 mag, we concluded that the completeness limit of the V magnitudes corresponds to this magnitude. This analysis shows that any cal-

Table 3: Photometric and astrometric catalogue for the open cluster NGC 225. The complete table can be obtained electronically.

ID	α_{2000} (hh:mm:ss.ss)	δ_{2000} (dd:mm:ss.ss)	V (mag)	$U-B$ (mag)	$B-V$ (mag)	$\mu_\alpha \cos\delta$ (mas yr^{-1})	μ_δ (mas yr^{-1})	P (%)
1	00:42:26.59	61:51:47.54	17.741±0.025	0.826±0.092	1.025±0.040	−1.3±3.9	−5.8±3.9	50
2	00:42:26.65	61:55:04.98	18.272±0.039	0.313±0.107	1.010±0.061	+27.6±4.0	−0.1±4.0	0
3	00:42:26.66	61:53:14.07	17.705±0.024	0.291±0.054	0.777±0.035	+18.0±4.0	+3.2±4.0	0
4	00:42:26.73	61:50:27.96	18.129±0.034	–	1.933±0.088	0.0±3.8	−1.3±3.8	69
5	00:42:26.75	61:46:04.52	17.657±0.024	0.326±0.082	1.375±0.043	−25.2±5.2	−21.1±5.2	0
–	–	–	–	–	–	–	–	–
–	–	–	–	–	–	–	–	–
–	–	–	–	–	–	–	–	–

Table 4: Mean errors of the photometric measurements for the stars in the field of NGC 225. N indicates the number of stars within the V apparent magnitude range given in the first column.

Mag. Range	N	σ_V	σ_{U-B}	σ_{B-V}
$9 < V \leq 11$	14	0.002	0.002	0.002
$11 < V \leq 13$	21	0.002	0.004	0.003
$13 < V \leq 14$	25	0.002	0.005	0.003
$14 < V \leq 15$	41	0.004	0.011	0.006
$15 < V \leq 16$	75	0.007	0.023	0.011
$16 < V \leq 17$	116	0.012	0.050	0.021
$17 < V \leq 18$	274	0.023	0.110	0.043
$18 < V \leq 19$	374	0.046	0.209	0.097
$19 < V \leq 20$	79	0.077	0.286	0.163

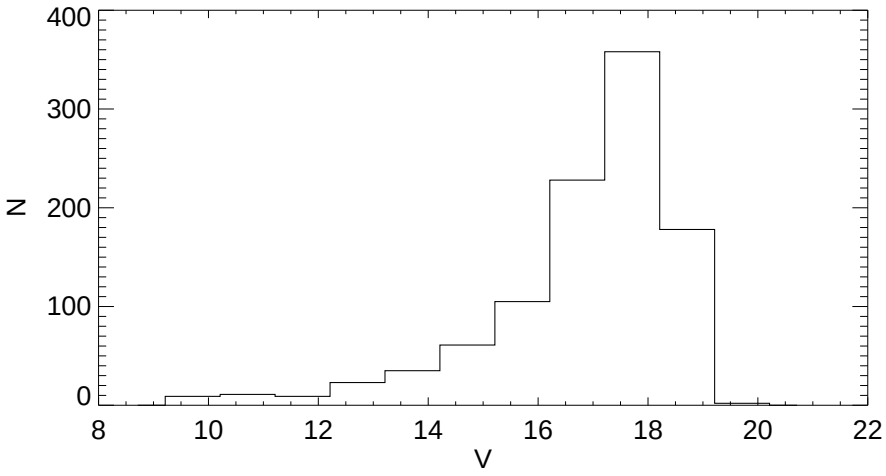

Figure 5: Histogram of the V-band magnitudes measured in the field of the open cluster NGC 225.

culation including only stars brighter than $V = 18$ mag in our catalogue will give reliable results for the cluster. The number of the stars with $V \leq 18$ mag in our catalogue is 566. Note that, although we found the photometric completeness limit for the stars in our V-band observations, this limit might not represent the brightnesses of the cluster stars. That is, most of the cluster stars can be much brighter or fainter than this completeness limit. Further analysis, which is given in the following section, is needed to conclude if the majority of the cluster's stars are fainter or brighter than the completeness limit of our catalogue.

3.2. Cluster radius and radial stellar surface density

It is well-known that the structural parameters of a cluster are calculated by counting the number of stars in different annuli around the center of the cluster. First, the stellar density in an area defined by a circle centered on the central coordinates of the cluster is calculated. From this central circle, the variation of stellar density within annuli with selected widths are calculated. These calculations of the stellar density are used to plot the stellar density profile, i.e. angular distance from the centre vs the stellar density. Finally, the density profile is fitted with the King (1962) model defined as,

$$\rho(r) = f_{bg} + \frac{f_0}{1 + (r/r_c)^2}, \quad (1)$$

where r represents the radius of the cluster centered at the celestial coordinates: $\alpha_{2000.0} = 00^h43^m39^s, \delta_{2000.0} = +61°46'30''$. f_{bg}, f_0 and r_c denote the background stellar density, the central stellar density and the core radius of the cluster, respectively. However, this method might not give reliable results for a bright and sparse cluster like NGC 225 due to contamination from background stars. Thus, we followed a different approach to find the most representative stellar density profile for the cluster with the assumption that the density profile of the cluster best fits with the King model. In order to do this, we plotted the density profiles of NGC 225 for the limiting V-band magnitudes of 15, 16, 17 and 18 and fitted each of them with the King model. These density profiles and the best fits are shown in Fig. 6. Note that the number of stars is very small for the limiting V-band magnitudes brighter than 15 mag. Using a χ^2 minimization technique, we found that the best fitted density profile is obtained for the limiting magnitude $V = 15$. The f_{bg}, f_0 and r_c were derived using this technique, as well. It should be noted that the central coordinates of the cluster were assumed to be as given in the WEBDA database. The increase in density near 8 arcmin from the center of the cluster (Fig. 6) is due to the contamination of faint field stars. Each panels in Fig. 6 shows the number of stars brighter than given V-magnitude. So, as the brightness limit goes to fainter magnitudes, fainter and fainter background stars are included in the consecutive panels. As a result, we face with a cumulative effect. As it can be seen, the effect of these fainter field stars increases to the fainter brightness limits. The weakest effect from the fainter field stars is found for $V < 15$ mag. This increase in the density demonstrates that the cluster stars have generally bright apparent magnitudes and the cluster has a sparsely distributed structure.

From this fit, we derived the central stellar density and core radius of the cluster, together with the background stellar density as $f_0 = 0.58 \pm 0.01$ stars arcmin^{-2}, $r_c = 1.99 \pm 0.08$ arcmin and $f_{bg} = 0.12 \pm 0.01$ stars arcmin^{-2}, respectively. The core radius derived in this study is smaller than $\sim$5 arcmin estimated by Lattanzi et al. (1991). An inspection of Fig. 6 by eye shows that the stellar density of the cluster is almost equal to that of the stellar background at about $r = 5$ arcmin from the center of the cluster. This analysis also shows that majority of confirmed members in the cluster are brighter than $V = 15$ mag.

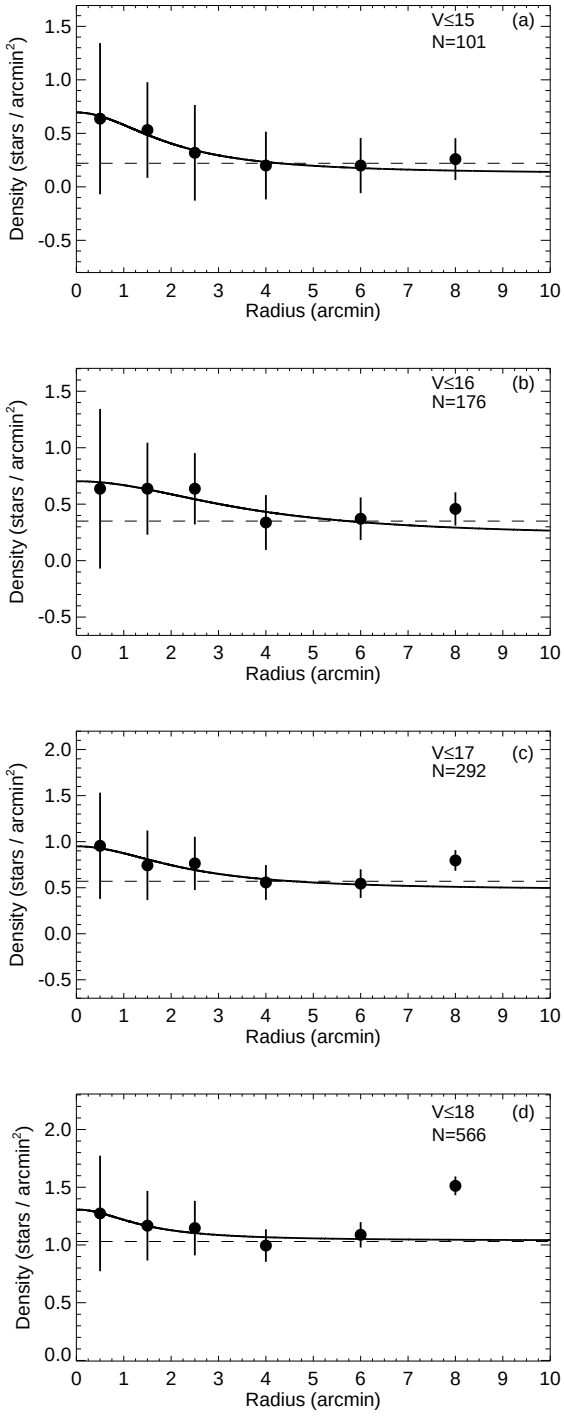

Figure 6: The stellar density profiles of NGC 225 plotted for the limiting V-band magnitudes 15 (a), 16 (b), 17 (c) and 18 (d). Solid lines represent the best fitted King model for each density profile. Errors were determined from sampling statistics: $1/\sqrt{N}$, where N is the number of stars used in the density estimation. Dashed lines represent the stellar density estimated using the stars with $P \leq 50\%$, which corresponds to the background level.

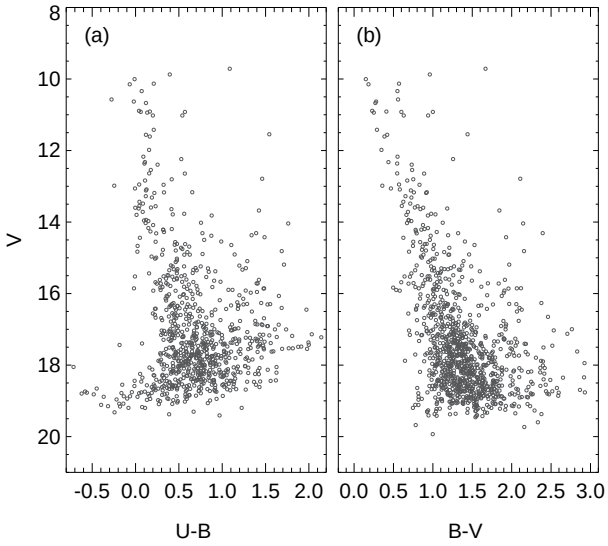

Figure 7: The CMDs for the cluster NGC 225. (a) V vs $U-B$, (b) V vs $B-V$.

3.3. CMDs and membership probabilities

The V vs $U-B$ and V vs $B-V$ CMDs of NGC 225 were constructed to derive the cluster's astrophysical parameters. The CMDs of the cluster are shown in Fig. 7. The cluster's main-sequence stars and a few giant stars can be distinguished by eye although the cluster is rather sparsely populated. The turn-off point with a small group of bright and blue stars in the CMDs of the cluster is located in $10 < V < 11$ mag.

One should be careful to determine whether giants and the main-sequence stars near the turn-off point of the CMDs are physical members of the cluster or not, before using them in the estimation of the astrophysical parameters of the cluster. Identification of the likely members of the cluster can also be useful for the determination of NGC 225's main-sequence. Thus, we calculated the probabilities (P) of the stars in the field being physical members of the cluster using a method described by Balaguer-Núnez et al. (1998). In this non-parametric method, we take into account both the errors of the mean cluster and the stellar proper motions, and determine the cluster and field stars' distributions empirically without any assumption about their shape. To derive the data distributions, we used the kernel estimation technique (with a circular Gaussian kernel function). The proper motions of the stars

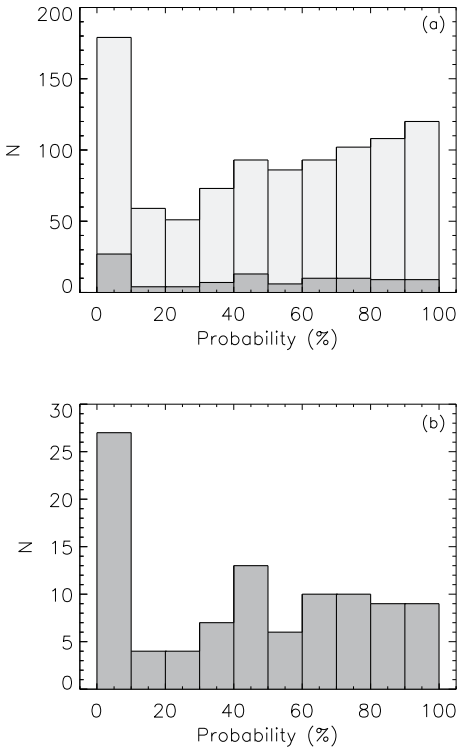

Figure 8: (a) Histogram of the membership probabilities of the stars in our catalogue for the magnitude ranges $10 \leq V \leq 19$ (light shaded bars) and $10 \leq V \leq 15$ mag (shaded bars). (b) Histogram of the membership probabilities of the stars in the magnitude range $10 \leq V \leq 15$ mag is shown in a larger scale.

in the CCD field were taken from the PPMXL Catalog of Roeser et al. (2010). Considering rectangular coordinates of the stars in the field, measured in two epochs, first our observations and second the ones obtained from Roeser et al. (2010), we compared our results with those of the algorithm published by Javakhishvili et al. (2006) and found excellent agreement. The histogram of the differences efficiently discriminate the members of the cluster from the non-members. The membership probabilities of the stars identified in the field of NGC 225 are listed in the last column of Table 3.

In order to determine the most likely members of the cluster, we first plotted the histogram of membership probabilities for the V-band magnitudes

of 1019 stars identified in the field of NGC 225. We also overplotted this histogram with the one constructed for the stars, whose apparent magnitudes are $10 \leq V \leq 15$ which is shown with grey bars in Fig. 8a. The above analysis about the structural parameters show that the majority of the cluster's member stars are in this magnitude range. In addition, the magnitude $V = 10$ roughly corresponds to the turn-off point of the cluster. The number of stars with $10 \leq V \leq 15$ mag in our catalogue is only 101. Their histogram is presented in Fig. 8b. Median value of the membership probabilities of these stars corresponds to $\sim$50%. Thus, we concluded that the stars with $P \geq 50\%$ are likely members of the cluster.

The zero age main-sequence (ZAMS) of Sung et al. (2013) for solar metallicity could be used to determine the most likely members of NGC 225 on the main-sequence. Thus, we fitted this ZAMS to the V vs $B-V$ CMD of the cluster for $10 \leq V \leq 15$ mag using only the stars with $P \geq 50\%$. By shifting the fitted main-sequence to brighter V magnitudes by 0.75 mag (see Fig. 9), a band like region in the V vs $B-V$ CMD was obtained to cover the binary stars, as well. Hence, we assumed that all stars with a membership probability $P \geq 50\%$ and located within this band-like region are the most likely main-sequence members of NGC 225, resulting in 28 stars. A visual inspection in Fig. 9 indicates that there are stars with $P \geq 50\%$ that have already left the ZAMS as shown by the red dots outside the main-sequence band. We assume that they are also likely members of the cluster. With this procedure, we identified 31 stars for further analyses.

4. Determination of the astrophysical parameters of NGC 225

4.1. The reddening

Interstellar reddening affects the TCDs and CMDs, from which the remaining astrophysical parameters will be determined. Thus, the colour excesses $E(U-B)$ and $E(B-V)$ must be inferred first. For the determination of these colour excesses, we used the most probable 28 main-sequence stars in the $10 \leq V \leq 15$ apparent magnitude range, which were selected according to the procedure in Section 3.3. The positions of these stars in the $U-B$ vs $B-V$ TCD were compared with the ZAMS of Sung et al. (2013) with a solar metallicity. In order to do this, the de-reddened main-sequence curve of Sung et al. (2013) was shifted with steps of 0.001 mag within the range $0 \leq E(B-V) \leq 0.60$ mag until the best fit is obtained with the $U-B$ vs

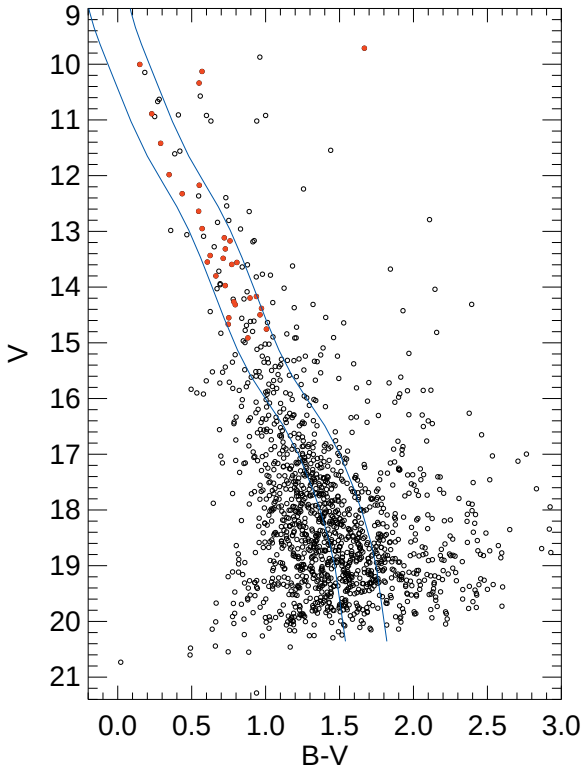

Figure 9: V vs $B-V$ CMD of NGC 225 constructed using all stars in our catalogue. Solid lines represent the ZAMS of Sung et al. (2013) and the one shifted by an amount of 0.75 mag to the bright V magnitudes. Red dots indicate the most probable cluster stars that are identified using a procedure explained in the text.

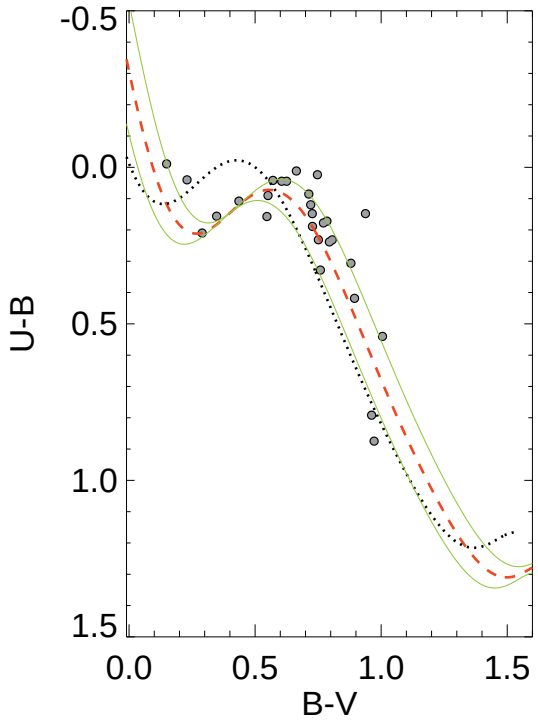

Figure 10: $U-B$ vs $B-V$ TCD for the main-sequence stars with $10 \leq V \leq 15$ mag in NGC 225. The reddened and de-reddened main-sequence curves (Sung et al., 2013) fitted to the cluster stars are represented with red dashed and black dotted lines, respectively. Green lines represent $\pm 1\sigma$ deviations. The number of stars is 28.

$B-V$ TCD of NGC 225. The shift in the $U-B$ axis was calculated by adopting the following equation (Cox, 2000):

$$E(U-B) = E(B-V) \times [0.72 + 0.05 \times E(B-V)]. \quad (2)$$

We show the $U-B$ vs $B-V$ TCD of NGC 225 for the most probable main-sequence stars of the cluster in Fig. 10. The goodness of the fit was determined by adopting the minimum χ^2 method. Using this method, we estimated the following colour excesses: $E(U-B) = 0.110 \pm 0.034$ and $E(B-V) = 0.151 \pm 0.047$ mag. The errors indicate the $\pm 1\sigma$ deviations.

4.2. Photometric metallicity of NGC 225

The metallicity of NGC 225 has not been determined in previous studies. We used the method described in Karaali et al. (2003, 2005, 2011) to measure the photometric metallicity. The procedure in this method uses F-G type main-sequence stars of the cluster. Thus, we selected 9 of 28 stars with colours $0.3 \leq (B-V)_0 \leq 0.6$ mag corresponding to F0-G0 spectral type main-sequence stars (Cox, 2000).

The difference between a star's de-reddened $(U-B)_0$ colour indice and the one corresponding to the members of the Hyades cluster with the same de-reddened $(B-V)_0$ colour index is the normalized UV excess of the star in question, i.e. $\delta = (U-B)_{0,H} - (U-B)_{0,S}$. Here, the subscripts H and S refer to Hyades and star, respectively. In order to utilize the method described in Karaali et al. (2011), we calculated the normalized UV excesses of the nine stars selected as described above and normalized their δ differences to the UV-excess at $(B-V)_0 = 0.6$ mag, i.e. $\delta_{0.6}$. The $(U-B)_0$ vs $(B-V)_0$ TCD and the histogram of the normalized UV excesses ($\delta_{0.6}$) of the selected nine main-sequence stars of NGC 225 are presented in Fig. 11. By fitting a Gaussian to this histogram, we calculated the normalized UV excess of the cluster as $\delta_{0.6} = 0.051 \pm 0.002$ mag. Here, the uncertainty is given as the statistical uncertainty of the peak of the Gaussian. Then, we estimated the metallicity ($[Fe/H]$) of the cluster by evaluating this Gaussian peak value in the following equation of Karaali et al. (2011):

$$[Fe/H] = -14.316(\pm 1.919)\delta_{0.6}^2 - 3.557(\pm 0.285)\delta_{0.6} + 0.105(\pm 0.039). \quad (3)$$

The metallicity corresponding to the peak value for the $\delta_{0.6}$ distribution was calculated as $[Fe/H] = -0.11 \pm 0.01$ dex. In order to transform the $[Fe/H]$ metallicity obtained from the photometry to the mass fraction Z, the following relation was used (Mowlavi et al., 2012):

$$Z = \frac{0.013}{0.04 + 10^{-[Fe/H]}}. \quad (4)$$

Here, Z is the mass fraction of all elements heavier than helium, which is used to estimate the theoretical stellar evolutionary isochrones. Hence, we calculated $Z = 0.009$ from the metallicity ($[Fe/H] = -0.11$ dex) obtained from the photometry. This metallicity will be used for the further analysis in this study.

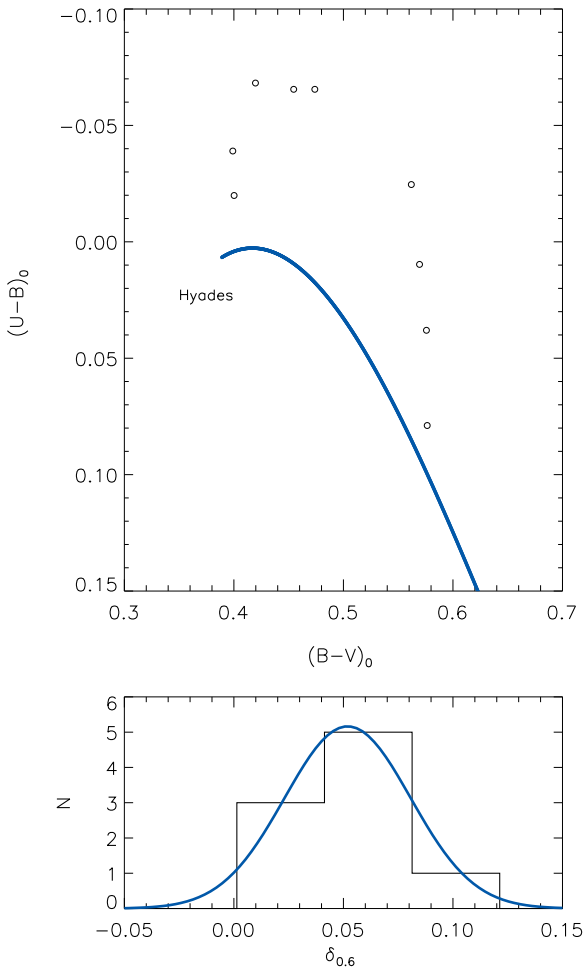

Figure 11: The $(U-B)_0$ vs $(B-V)_0$ TCD (upper panel) and the histogram (lower panel) for the normalized UV-excesses for nine main-sequence stars used for the metallicity estimation of NGC 225. The solid lines in the upper and lower panels represent the main-sequence of Hyades cluster and the Gaussian fit of the histogram, respectively.

Table 5: Colour excesses, metallicities (Z), distance moduli (μ), distances (d) and ages (t) estimated using two CMDs of NGC 225.

CMD	Colour Excess (mag)	Z	μ_V (mag)	d (pc)	t (Myr)
V vs $U-B$	$E(U-B)=0.110\pm0.034$	0.009	9.30 ± 0.07	585 ± 20	900 ± 100
V vs $B-V$	$E(B-V)=0.151\pm0.047$	0.009	9.30 ± 0.07	585 ± 20	900 ± 100

4.3. Distance modulus and age of NGC 225

We fitted the V vs $U-B$ and V vs $B-V$ CMDs of the cluster with the theoretical isochrones provided by the PARSEC synthetic stellar library (Bressan et al., 2012), which was recently updated (PARSEC version 1.2S, Tang et al., 2014; Chen et al., 2014) to derive the distance modula and age of NGC 225 simultaneously. Since the reddening and metallicity of the cluster were above determined using its $(U-B)_0$ vs $(B-V)_0$ TCD and the normalized ultraviolet (UV) excesses of the cluster members, respectively, we kept the metallicity and the reddening as constants during the fitting process. As already noted in Yontan et al. (2015) and Bostancı et al. (2015), the measured reddening, metallicity, and therefore the age values can suffer from the degeneracies between the parameters when these parameters are determined simultaneously. Thus, uncertainty of the age and reddening can be higher than expected from the simultaneous solutions. To overcome this problem, we determined the metallicity and reddening of the cluster using independent and reliable methods and kept these parameters as constants in the analysis. We expect that the degeneracy/indeterminacy of the parameters determined in this study will be less than that in the statistical solutions with four free astrophysical parameters (i.e. the reddening, distance modulus, metallicity and age).

The estimated astrophysical parameters of NGC 225 obtained from the best fits to the CMDs are given in Table 5. Errors of the parameters were derived by visually shifting the theoretical isochrones to include all the main-sequence stars in the CMDs. The best fit theoretical isochrones for $Z=0.009$ and $t=900$ Myr in the V vs $B-V$ and V vs $U-B$ CMDs are overplotted in Fig. 12.

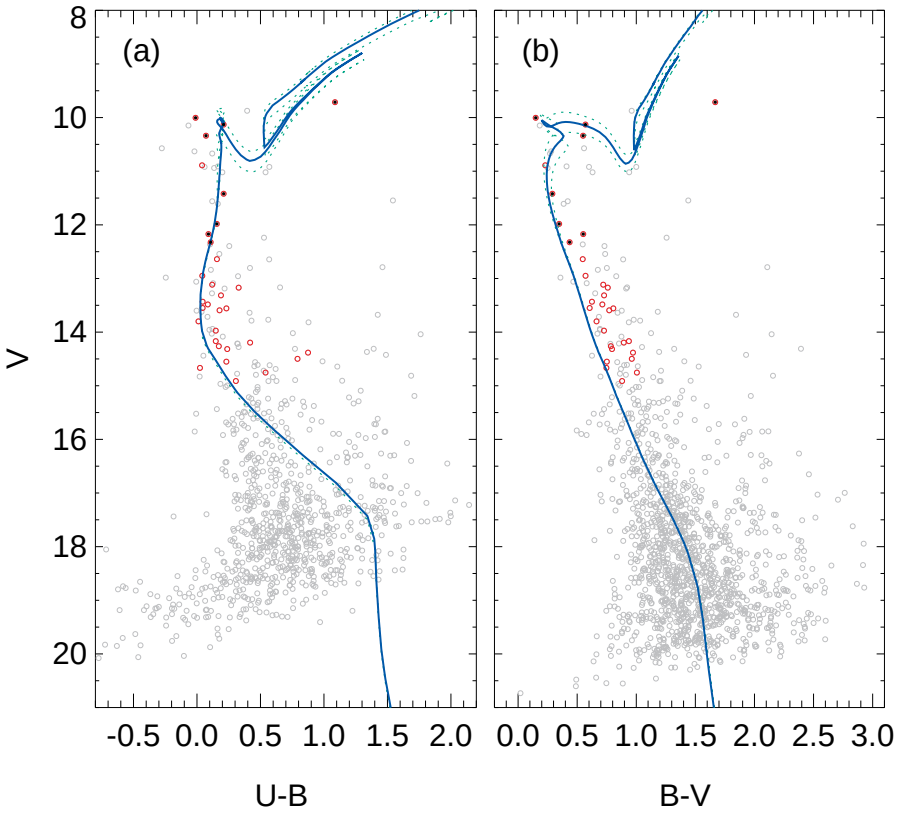

Figure 12: V vs $U-B$ (a) and V vs $B-V$ (b) CMDs for the stars in the field of NGC 225. The most probable members of the cluster are indicated with red circles. These stars are fitted to the isochrone determined in this study (blue line). The green dots indicate the isochrones with estimated age plus/minus its error. Stars indicated with black dotes are the ones with spectra from which RVs were measured in this work.

Table 6: The data for stars used in the calculation of the galactic orbit and space velocity components of NGC 225. LMM 88 is a spectroscopic binary star which was not used in these calculations. V_r denotes the radial velocity measured from the spectra in this study. Star names were taken from the SIMBAD Database.

Star	α_{2000} (hh:mm:ss.ss)	δ_{2000} (dd:mm:ss.ss)	V (mag)	$B-V$ (mag)	$\mu_\alpha \cos\delta$ (mas yr^{-1})	μ_δ (mas yr^{-1})	V_r (km s^{-1})	P (%)
LMM 83	00 43 10.86	+61 47 18.96	10.130 ± 0.002	0.570 ± 0.002	-2.7 ± 2.0	-1.8 ± 2.0	-6.6	64
LMM 94	00 43 26.59	+61 45 55.82	10.338 ± 0.002	0.550 ± 0.002	-4.0 ± 2.0	$+0.6 \pm 2.0$	-4.0	96
LMM 96	00 43 30.99	+61 48 10.25	12.172 ± 0.001	0.551 ± 0.002	-4.8 ± 2.0	-1.0 ± 2.0	-13.4	92
LMM 98	00 43 36.93	+61 53 40.08	11.982 ± 0.005	0.347 ± 0.006	-6.2 ± 2.0	$+2.4 \pm 2.0$	-7.1	67
LMM 114	00 43 51.48	+61 47 13.43	10.890 ± 0.002	0.230 ± 0.001	-3.8 ± 2.0	-2.2 ± 2.0	0.4	69
LMM 127	00 44 12.80	+61 51 01.89	11.420 ± 0.003	0.290 ± 0.004	-5.9 ± 2.0	$+1.3 \pm 2.0$	-17.4	86
LMM 132	00 44 16.55	+61 50 44.05	12.324 ± 0.001	0.436 ± 0.002	-6.8 ± 2.0	-0.3 ± 2.0	-16.1	77
LMM 170	00 44 46.42	+61 52 31.44	10.004 ± 0.001	0.149 ± 0.001	-5.4 ± 2.0	$+1.7 \pm 2.0$	-2.4	86

4.4. Galactic orbit of the cluster

The procedure of estimating the galactic orbital parameters of an object is described in Dinescu et al. (1999), Coşkunoğlu et al. (2012) and Bilir et al. (2012). To estimate galactic orbital parameters of NGC 225, we first performed a test-particle integration in a Milky Way potential which consists of a logarithmic halo, a Miyamoto-Nagai potential to represent the galactic disc and a Hernquist potential to model the bulge.

We calculated galactic orbits of the eight cluster stars with a membership probability larger than 50% for which RV data are given in Table 6. Mean values of the RV, proper motion components of these stars and the distance of the cluster were taken as the input parameters for the cluster's galactic orbit estimation: $V_r = -8.3 \pm 5.0$ km s^{-1}, $\mu_\alpha \cos\delta = -4.95 \pm 2.0$ and $\mu_\delta = 0.09 \pm 2.0$ mas yr^{-1}, and $d = 585 \pm 20$ pc, respectively. Mermilliod et al. (2008) measured the RV of LMM 88 (BD+60 86) as -33.86 ± 0.76 km s^{-1}, which is very different than the value in Table 6. Therefore, this star was excluded from the calculation of the mean RV of the cluster, since it is probably a spectroscopic binary. The proper motion components were taken from Roeser et al. (2010), while the RVs of the cluster stars and their distances were found in this study. We determined galactic orbits of the stars within an integration time of 3 Gyr in steps of 2 Myr. This integration time corresponds to minimum 12 revolutions around the galactic center so that the averaged orbital parameters can be determined reliably.

In order to determine the galactic orbit of the cluster, we adopted means of the orbital parameters found for the stars as the orbital parameters of

the cluster. Fig. 13 shows the representations of galactic orbits calculated for the cluster stars and the cluster itself in the $X-Y$ and $X-Z$ planes. Here, X, Y and Z are heliocentric galactic coordinates directed towards the galactic centre, galactic rotation and the north galactic pole, respectively. We obtained the cluster's apogalactic (R_a) and perigalactic (R_p) distances as 9.37 ± 0.15 and 8.22 ± 0.12 kpc, respectively. The maximum vertical distance from the galactic plane is calculated as $Z_{max} = 90 \pm 70$ pc. We used the following formula in the determination of the eccentricity projected on to the galactic plane: $e = (R_a - R_p)/(R_a + R_p)$. The eccentricity of the orbit was calculated as $e = 0.07 \pm 0.01$. This value shows that the cluster is orbiting the Galaxy with a period of $P_{orb} = 255 \pm 5$ Myr on nearly circular orbit as expected for the objects in the solar neighbourhood.

We also computed the galactic space velocity components of the stars in Table 6 with respect to the Sun using the algorithms and transformation matrices of Johnson & Soderblom (1987). The input data in Table 6 are in the form adopted for the epoch of J2000 as described in the International Celestial Reference System (ICRS) of *Hipparcos* and Tycho Catalogues (ESA, 1997). The calculated space velocity components are $(U, V, W) = (16.02 \pm 5.41, 0.25 \pm 5.17, 0.82 \pm 5.55)$ km s^{-1}. The uncertainties of these components were computed by propagating the uncertainties of the input data (proper motions, distance and RV) with an algorithm also by Johnson & Soderblom (1987). We applied corrections for the differential galactic rotation to the space velocity components as described in Mihalas & Binney (1981). We also corrected the galactic space velocity components for the Local Standard of Rest (LSR) by adding the space velocity of the Sun to the space velocity components of the stars. The adopted space velocity of the Sun is $(U, V, W) = (8.50, 13.38, 6.49)$ km s^{-1} (Coşkunoğlu et al., 2011). We adopted means of the space velocity components found for the stars as the space velocity components of the cluster. Finally, the corrected space velocity components of NGC 225 were found as $(U, V, W) = (11.03 \pm 5.41, 14.37 \pm 5.17, 7.31 \pm 5.55)$ km s^{-1}. We estimated the total space velocity of the cluster as $S_{tot} = 19.53 \pm 9.32$ km s^{-1}, which is in agreement with the one suggested for the young thin-disc stars and young stellar clusters (Leggett, 1992).

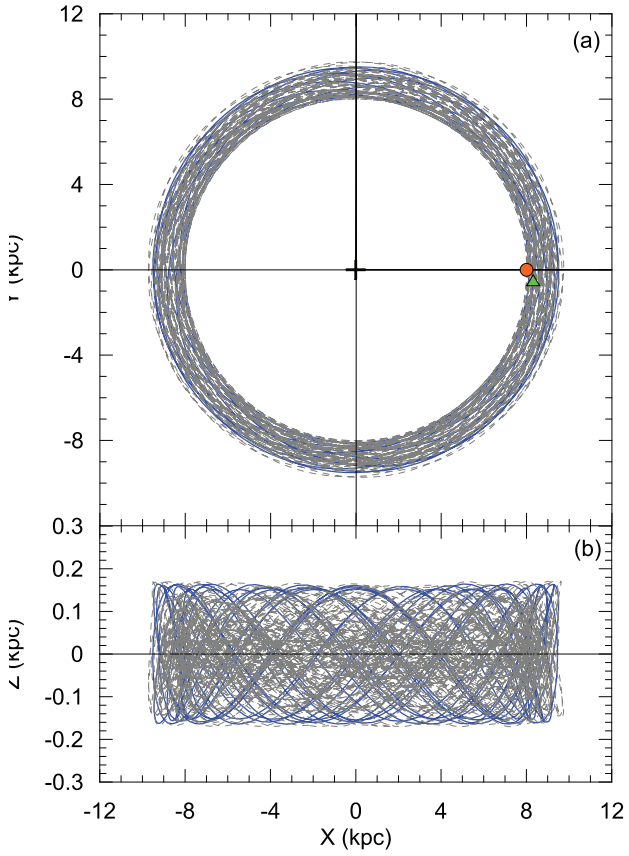

Figure 13: The galactic orbital motions (grey dashed lines) of eight cluster stars with P $\geq$ 50%, for which RVs are available, in the $X-Y$ (a) and $X-Z$ (b) planes. The cluster's mean orbit is indicated with a blue line. The black plus, red circle and green triangle symbols in panel (a) represent the galactic centre, and current locations of the sun and NGC 225, respectively.

5. Discussion

In this paper, we present the first CCD UBV photometry for the open cluster NGC 225. From these data, we determined structural and astrophysical parameters of the cluster. We also calculated the mean RV of the cluster from the spectroscopic observations of the cluster members. Using the proper motions of the stars in the field, we estimated probability of the stars in the cluster field being physical members of the cluster. We also calculated the space velocity components and the parameters of the galactic orbit of NGC 225.

Independent methods developed for the determination of the reddening and metallicity were used in this study to reduce the number of free parameters in the simultaneous solutions, where the theoretical stellar evolutionary isochrones are fitted to the observed CMDs, since the astrophysical parameters of a cluster suffer from the reddening-age degeneracy when all of them (the reddening, metallicity, distance modulus and the age) are simultaneously determined by this fitting process (cf. Anders et al., 2004; King et al., 2005; Bridźius et al., 2008; de Meulenaer et al., 2013). Thus, we inferred the reddening of the open cluster NGC 225 from its $U-B$ vs $B-V$ TCD, while we determined the metallicity of the cluster utilizing F0-G0 spectral type main-sequence stars (Cox, 2000) via a metallicity calibration defined by Karaali et al. (2011). The reddening and metallicity of the cluster obtained from the UBV photometric data are $E(B-V) = 0.151 \pm 0.047$ mag and $[Fe/H] = -0.11 \pm 0.01$ dex ($Z = 0.009$), respectively. This is the first determination of the metallicity for NGC 225. While keeping the reddening and metallicity constant, we inferred the distance modulus and age of the cluster as $(m-M) = 9.30 \pm 0.07$ mag and $t = 900 \pm 100$ Myr, respectively, by fitting the theoretical isochrones to the observed CMDs. From the estimated distance modulus and the colour excess, we find the distance of NGC 225 as $d = 585 \pm 20$ pc, which is in agreement with that found by Lattanzi et al. (1991) within errors. A comparison of the reddening values with those estimated in previous studies shows that the colour excess obtained in this study is smaller than $E(B-V) = 0.29$ mag given by Johnson et al. (1961) and Svolopoulos (1962), while it is in agreement roughly with $E(B-V) = 0.25 \pm 0.08$ mag found by Lattanzi et al. (1991) within errors. The distance modulus obtained in this study $(m-M) = 9.30 \pm 0.07$ mag is in agreement with the previous estimates of $(m-M) = 9.0$ and $(m-M) = 9.1$ mag (Svolopoulos, 1962; Hoag & Applequist, 1965) within

errors, as well.

We compared the spectral types and membership probabilities estimated in our study with those in Lattanzi et al. (1991). The comparison is shown in Table 7. Stars in the Table 7 are indicated as the most probable members of the cluster by Lattanzi et al. (1991). An inspection by eye shows that spectral types and membership probabilites in the two studies are generally in agreement. Differences between the probabilites are due to the proper motion accuracies of the catalogues used in the two studies. Since we have taken the proper motion values from Roeser et al. (2010), proper motion errors in our study are smaller than those in Lattanzi et al. (1991), indicating that the membership estimated in our study are more reliable.

As for the age of NGC 225, Lattanzi et al. (1991) estimated the age of the cluster as $t = 120$ Myr, while Subramaniam et al. (2006) argued that the age should be $t = 0.5 - 10$ Myr based on pre-main sequence isochrones. However, we found age of the cluster to be much older than both determinations as $t = 900 \pm 100$ Myr by fitting the theoretical isochrones provided by the PARSEC synthetic stellar library (Bressan et al., 2012), which was recently updated (PARSEC version 1.2S, Tang et al., 2014; Chen et al., 2014), to the observed V vs $U-B$ and V vs $B-V$ CMDs in this study. Subramaniam et al. (2006) show that there are eight stars with H_α emission located around the cluster, of which two are probable Herbig Be stars (LKH_α 201 and BD +61 154) located within the cluster's field. According to Subramaniam et al. (2006), these two stars indicate that the age of NGC 225 is 1.5−3.0 Myr, if they are members of the cluster. The re-reduced *Hipparcos* parallax of BD +61 154 is $\pi = 4.96 \pm 1.61$ mas (van Leeuwen, 2007). This value compares to the cluster's parallax (1.71 ± 0.06 mas) only within 2σ error level. It should be noted that the GAIA observations will reveal if this star is a member of the cluster. Subramaniam et al. (2006) calculated the distance of LKH_α 201 as $d = 1500$ pc and showed that the star is behind the cluster. So, LKH_α 201 is not a member of NGC 225, as well. Thus, we conclude that presence of these stars in the field of the cluster is just a coincidence.

In addition, LKH_α 200 was also used by Subramaniam et al. (2006) to show that the cluster is very young. However, the membership probabilities of LKH_α 200 and LKH_α 201 are estimated to be 0% in our study as well as in Lattanzi et al. (1991) (see Table 7). Thus, LKH_α 200 can not be used in the estimation of the cluster's age, as well.

Table 7: Comparison of the photometry, spectral types and membership probabilities given in Lattanzi et al. (1991) and this study.

			Lattanzi et al. (1991)						This Study					
ID	α_{2000} (hh:mm:ss.ss)	δ_{2000} (dd:mm:ss.ss)	Star	Star	SpT	V (mag)	$B-V$ (mag)	P (%)	SpT	V (mag)	$U-B$ (mag)	$B-V$ (mag)	P (%)	Remark
01	00:42:12.40	61:38:16.49	LMM 29	—	F8	13.44	0.67	58	—	—	—	—	—	out of FoV
02	00:42:17.90	61:59:35.94	LMM 33	—	F	12.55	0.57	93	B4V	—	—	—	—	out of FoV
03	00:42:29.37	61:55:46.66	LMM 49	LkHA 200	K3Ve	13.47	0.29	00	—	14.020	0.755	1.125	00	
04	00:42:34.46	61:54:01.13	LMM 55	—		15.27	0.73	63	—	15.522	-0.007	0.640	27	
05	00:43:05.53	61:53:43.83	LMM 77	—	F8	13.52	0.65	90	—	13.484	0.085	0.713	99	
06	00:43:07.27	61:46:27.41	LMM 80	—		13.64	0.87	96	—	13.600	-0.003	0.877	09	
07	00:43:25.33	61:38:23.30	LMM 91	LkHA 201	B2e	14.32	1.29	00	—	13.621	0.036	1.182	00	
08	00:43:25.65	61:48:51.68	LMM 92	—	A2	11.51	0.44	78	B9IV	11.560	0.120	0.420	43	
09	00:43:26.59	61:45:55.82	LMM 94	BD+60 87	B9	10.25	0.62	93	B8IV	10.338	0.071	0.550	96	
10	00:43:28.87	61:48:04.10	LMM 95	—	A0	10.89	0.29	94	A0IV	10.940	0.135	0.250	42	
11	00:43:30.99	61:48:10.25	LMM 96	—	A7	12.22	0.58	69	A5V	12.172	0.090	0.551	92	
12	00:43:36.93	61:53:40.08	LMM 98	—	A5	12.04	0.36	94	A4V	11.982	0.156	0.347	67	
13	00:43:51.06	61:50:08.21	LMM 113	BD+61 157	A0	10.64	0.24	94	B9V	10.630	-0.020	0.280	49	
14	00:43:51.48	61:47:13.43	LMM 114	—	A1	10.92	0.20	86	B9V	10.890	0.040	0.230	69	
15	00:44:07.49	61:42:51.94	LMM 123	—		13.63	0.93	94	—	13.639	0.414	0.842	00	
16	00:44:12.80	61:51:01.89	LMM 127	—	A3	11.43	0.28	92	A0V	11.420	0.210	0.290	86	
17	00:44:16.55	61:50:44.05	LMM 132	—	A7	12.39	0.41	75	A5V	12.324	0.108	0.436	77	
18	00:44:20.76	61:49:45.15	LMM 136	—	F6	13.14	0.75	54	—	13.116	0.120	0.720	01	
19	00:44:30.68	61:46:49.94	LMM 149	BD+60 94	B8	9.73	0.17	94	B8V	—	—	—	—	saturation
20	00:44:38.17	61:45:06.82	LMM 157	BD+60 95	B9	10.23	0.19	00	—	10.148	-0.067	0.183	03	
21	00:44:40.46	61:54:01.77	LMM 161	BD+61 162	B9	9.67	0.14	93	B9V	—	—	—	—	saturation
22	00:44:40.82	61:48:43.32	LMM 163	BD+61 163	B6.5	9.35	0.04	93	B7IV-V	—	—	—	—	saturation
23	00:44:46.42	61:52:31.44	LMM 170	BD+61 164	A0	10.03	0.08	75	B9V	10.004	-0.011	0.149	86	
24	00:44:47.45	61:56:49.16	LMM 174	—	A3	11.58	0.47	52	A3IV	11.982	0.156	0.347	67	
25	00:45:08.36	61:56:24.49	LMM 197	—	A7	12.52	0.55	71	A7III-IV	12.984	-0.246	0.358	34	
26	00:45:18.73	61:46:17.77	LMM 213	—		14.66	0.65	62	—	—	—	—	—	out of FoV
27	00:45:26.34	61:38:53.30	LMM 219	LkHA 205		14.39	1.49	00	—	—	—	—	—	out of FoV
28	00:45:49.70	61:42:43.63	LMM 253	—		15.25	1.21	67	—	—	—	—	—	out of FoV
29	00:45:55.02	61:54:30.16	LMM 260	—	G5	14.61	1.60	77	—	—	—	—	—	out of FoV
30	00:46:03.23	61:52:17.76	LMM 270	—	G-K	14.62	1.47	70	—	—	—	—	—	out of FoV
31	00:46:04.53	61:44:38.04	LMM 271	—		14.32	0.76	51	—	—	—	—	—	out of FoV

The RVs of a considerable number of stars in the direction of NGC 225 were measured for the first time in this study (Table 2). A mean RV of -8.3 ± 5.0 km s^{-1} was calculated for the cluster. A search in the literature for stars in Table 2 shows that there are only two stars, whose RVs were previously measured. Mermilliod et al. (2008) determined the RVs of LMM 88 (BD+60 86) and LMM 115 (BD+60 91) as -33.86 ± 0.76 km s^{-1} and -168.03 ± 0.26 km s^{-1}, respectively. Our RV measurement for LMM 115 ($V_r = -168.2 \pm 5.0$ km s^{-1}) is in a perfect agreement with that of Mermilliod et al. (2008), while an agreement between the two studies could not be found for LMM 88 ($V_r = -129.0 \pm 5.0$ km s^{-1}) as this star is likely a spectroscopic binary.

In order to determine the galactic orbit of the cluster, we adopted means of the galactic orbital parameters found for the cluster stars, whose RVs were obtained currently from their spectra, as the galactic orbital parameters of NGC 225. The maximum vertical distance from the galactic plane, eccentricity and period for the galactic orbit of NGC 225 were calculated as $Z_{max} = 90 \pm 70$ pc, $e = 0.07 \pm 0.01$ and $P_{orb} = 255 \pm 5$ Myr, respectively. Wu et al. (2009) calculated these parameters as $Z_{max} = 70 \pm 30$ pc, $e = 0.09 \pm 0.01$ and $P_{orb} = 227.7 \pm 4.5$ Myr which are in agreement with our estimates. We obtained the cluster's apogalactic and perigalactic distances as $R_a = 9.37 \pm 0.15$ and $R_p = 8.22 \pm 0.12$ kpc, respectively. We also computed the space velocity components of the cluster using the stars in Table 6. The space velocity components of NGC 225 with respect to the galactic centre were determined as $(U, V, W) = (16.02 \pm 5.41, 219.75.25 \pm 5.17, 0.82 \pm 5.55)$ km s^{-1} in this study, where the V component for galactic rotation velocity of the Sun ($V = 220$ km s^{-1}) was used as the correction term. Then, the total space velocity of the cluster is estimated $S_{tot} = 220$ km s^{-1}. Wu et al. (2009) calculated the uncorrected space velocity components of NGC 225 as $(U, V, W) = (38.0 \pm 3.3, 209.6 \pm 2.1, 6.6 \pm 0.4)$ km s^{-1} which give a total space velocity of $S_{tot} = 213$ km s^{-1}. These calculations show that our results about the galactic orbit of the cluster are in agreement with those found by Wu et al. (2009).

6. Acknowledgments

Authors are grateful to the anonymous referees for their useful comments and improvements for the manuscript. This work has been supported in part by the Scientific and Technological Research Council (TÜBİTAK) 113F270.

Part of this work was supported by the Research Fund of the University of Istanbul, Project Numbers: 39170 and 39582. We thank to TÜBİTAK National Observatory for a partial support in using T100 and RTT150 telescopes with project numbers 11BT100-180, 15AT100-738 and 09BRTT150-470. We also thank to the on-duty observers and members of the technical staff at the TÜBİTAK National Observatory for their support before and during the observations. This research has made use of the SIMBAD and "Aladin sky atlas" developed at CDS, Strasbourg Observatory, France, WEBDA and NASA's Astrophysics Data System Bibliographic Services. We made use of data from the UVES Paranal Observatory project (ESO DDT Program ID 266.D-5655).

References

Ak, T., Bostancı, Z.F., Yontan, T., Bilir, S., Güver, T., Ak, S., Ürgüp, H., & Paunzen, E. 2016, Ap&SS, 361, 126

Anders, P., Bissantz, N., Fritze-v Alvensleben, U., & de Grijs, R. 2004, MNRAS, 347, 196

Andreuzzi, G., Richer, H.B., Limongi, M., & Bolte, M. 2002, A&A, 390, 961

Bagnulo S., Jehin E., Ledoux C., Cabanac R., Melo C., Gilmozzi R., & ESO Paranal Science Operations Team 2003, The Messenger, 114, 10

Balaguer-Núnez, L., Tian, K.P., & Zhao, J.L. 1998, A&AS, 133, 387

Becker, W., & Fenkart, R. 1971, A&AS, 4, 241

Bertin, E., & Arnouts, S. 1996, A&AS, 117, 393

Bertin, E. 2011, ASPC, 442, 435

Bilir, S., Güver, T., Khamitov, I., Ak, T., Ak, S., Coşkunoğlu, K. B., Paunzen, E., & Yaz, E. 2010, Ap&SS, 326, 139

Bilir, S., Karaali, S., Ak, S., Önal, Ö., Dağtekin, N. D., Yontan, T., Gilmore, G., & Seabroke, G.M. 2012, MNRAS, 421, 3362

Bostancı, Z.F., Ak, T., Yontan, T., Bilir, S., Güver, T., Ak, S., Çakırlı, Ö., Özdarcan, O., Paunzen, E., De Cat, P., Fu, J.N., Zhang, Y., Hou, Y., Li, G., Wang, Y., Zhang, W., Shi, J., & Wu, Y. 2015, MNRAS, 453, 1095

Bressan, A., Marigo, P., Girardi, L., Salasnich, B., Dal Cero, C., Rubele, S., & Nanni, A. 2012, MNRAS, 427, 127

Bridžius, A., Narbutis, D., Stonkuté, R., Deveikis, V., & Vansevičius, V. 2008, BaltA, 17, 337

Chen, Y., Girardi, L., Bressan, A., Marigo, P., Barbieri, M., & Kong, X. 2014, MNRAS, 444, 2525

Coşkunoğlu, B., et al. 2011, MNRAS, 412, 1237

Coşkunoğlu, B., Ak, S., Bilir, S., Karaali, S., Önal, Ö., Yaz, E., Gilmore, G., & Seabroke, G. M. 2012, MNRAS, 419, 2844

Cox, A.N. 2000. Allen's astrophysical quantities, 4th ed. Publisher: New York: AIP Press; Springer, 2000. Edited by Arthur N. Cox. ISBN: 0387987460

de Meulenaer, P., Narbutis, D., Mineikis, T., & Vancevičius, V. 2013, A&A, 550, 20

Dinescu, D. I., Girardi, T.M., & van Altena, W. F. 1999, AJ, 117, 1792

ESA, 1997, The Hipparcos and Tycho catalogues. Publisher: Noordwijk, Netherlands: ESA Publications Division 1997, Series: ESA SP Series vol no: 1200, ISBN: 9290923997

Hoag, A.A., Johnson, H.L., Iriarte, B., Mitchell, R.I., Hallam, K.L., & Sharpless, S. 1961, Publications of the U.S. Naval Observatory, 2d ser., 17, 344

Hoag, A.A., & Applequist, N.L. 1965, ApJS, 12, 215

Janes, K., & Hoq, S. 2013, AJ, 141, 92

Javakhishvili, G., Kukhianidze, V., Todua, M., & Inasaridze, R. 2006, A&A, 447, 915

Johnson, H.L., Hoag, A.A., Iriarte, B., Mitchell, R.I., & Hallam, K.L. 1961, Lowell Observatory, Bulletin No. 113, V.5, No.8, 133

Johnson, D.R.H., & Soderblom, D.R. 1987, AJ, 93, 864

Karaali, S., Bilir, S., Karataş, Y., Ak, S. G., 2003, PASA, 20, 165

Karaali, S., Bilir, S., & Hamzaoğlu, E. 2004, MNRAS, 355, 307

Karaali, S., Bilir, S., & Tunçel, S. 2005, PASA, 22, 24

Karaali, S., Bilir, S., Ak, S., Yaz, E., & Coşkunoğlu, B. 2011, PASA, 28, 95

King, I. 1962, AJ, 67, 471

King, I.R., Bedin, L.R., Piotto, G., Cassisi, S., & Anderson, J. 2005, AJ, 130, 626

Landolt, A.U. 2009, AJ, 137, 4186

Lang, D. 2009, Thesis (Ph.D.), University of Toronto (Canada), ISBN: 9780494610008

Lattanzi, M.G., Massone, G., & Munari, U. 1991, AJ, 102, 177

Lee, O.J. 1926, MNRAS, 86, 645

Leggett, S.K. 1992, ApJS, 82, 351

Mermilliod, J.C., Mayor, M., & Udry, S. 2008, A&A, 485, 303

Mihalas, D., & Binney, J. 1981, In: Galactic Astronomy, second ed. Freeman, San Fransisco.

Mowlavi, N., Eggenberger, P., Meynet, G., Ekström, S., Georgy, C., Maeder, A., Charbonnel, C., & Eyer, L. 2012, A&A, 541, A41

Roeser, S., Demleitner, M., & Schilbach, E. 2010, AJ, 139, 2440

Skrutskie, M.F., et al. 2006, AJ, 131, 1163

Subramaniam, A., Mathew, B., Kartha, S.S., et al. 2006, BASI, 34, 315

Sung, H., Lim, B., Bessell, M.S., Kim, J.S., Hur, H., Chun, M., & Park, B. 2013, JKAS, 46, 103

Svolopoulos, S.N. 1962, ApJ, 136, 788

Tang, J., Bressan, A., Rosenfield, P., Slemer, A., Marigo, P., Girardi, L., & Bianchi, L. 2014, MNRAS, 445, 4287

van Leeuwen, F. 2007, A&A, 474, 653

Wu, Z.-Yu, Zhou, X., Ma, J., & Du, C.-H. 2009, MNRAS, 399, 2146

Yontan, T., Bilir, S., Bostancı, Z.F., Ak, T., Karaali, S., Güver, T., Ak, S., Duran, Ş., & Paunzen, E. 2015, Ap&SS, 355, 267